Natural Resources Canada | Ressources naturelles Canada

GEOLOGICAL SURVEY OF CANADA
OPEN FILE 7599

Petrography, mineralogy, and initial fluid-inclusion results from the Jason, Tom, and Nidd SEDEX deposits, Macmillan Pass District, Yukon

J.M. Magnall, S.A. Gleeson, S. Paradis, and N.J.F. Blamey

2017

GEOLOGICAL SURVEY OF CANADA
OPEN FILE 7599

Petrography, mineralogy and initial fluid-inclusion results from the Jason, Tom, and Nidd SEDEX deposits, Macmillan Pass District, Yukon

J.M. Magnall[1*], S.A. Gleeson[1*], S. Paradis[2], and N.J.F. Blamey[3]

[1] Department of Earth and Atmospheric Sciences, University of Alberta, Edmonton, Alberta T6G 2E3

* Current address: GeoForschungsZentrum Potsdam, Telegrafenberg, 14473 Potsdam, Germany

[2] Geological Survey of Canada, 9860 West Saanich Road, Sidney, British Columbia V8L 4B2

[3] Department of Earth Sciences, Brock University, 500 Glenridge Avenue, Ontario L2S 3A1

2017

doi:10.4095/301691

This publication is available for free download through GEOSCAN (http://geoscan.nrcan.gc.ca/).

Recommended citation
Magnall, J.M., Gleeson, S.A., and Paradis, S., and Blamey, N.J.F., 2017. Petrography, mineralogy, and initial fluid-inclusion results from the Jason, Tom, and Nidd SEDEX deposits, Macmillan Pass, Yukon; Geological Survey of Canada, Open File 7599, 31 p. doi:10.4095/301691

Publications in this series have not been edited; they are released as submitted by the author.

Table of Contents

ABSTRACT

Sediment-hosted base metal mineralization in the Selwyn Basin occurs during 3 time intervals in the Cambrian, Silurian and Late Devonian, coeval with magmatic episodes. At Macmillan Pass, the Tom, Jason and Nidd showings are hosted by Upper Devonian sediments and have well preserved vent complexes beneath overlying bedded sulphides (Tom, Jason).

Core was sampled from the vent complexes at Tom, Jason, and Nidd. Detailed petrography (reflected and transmitted light and cathodoluminescence), was conducted to characterize the mineralogy within the vent complex, and the relationship of fluid inclusion bearing mineral phases to base metal sulphides. Microthermometry (Tom and Nidd) and bulk incremental fast scan gas mass spectrometry (Nidd) was performed on fluid inclusion samples. Carbon, oxygen and sulphur isotopes were analysed on mineral separates to determine the source of these components in each system.

The petrography indicates that for all three localities, fluid flow in the vent can be split in two distinct stages. Stage 1 is dominated by extensive stock-work style iron carbonate veining, along with destructive carbonate and pyrite alteration. Base-metal sulphides are deposited during Stage 2, in association with a volumetrically minor gangue assemblage (siderite, quartz ± barite, barytocalcite and quartz). Initial fluid inclusion results indicate the presence of a CO_2-bearing assemblage at Nidd, which has preserved evidence of phase immiscibility. The N_2-Ar-He bulk composition of these samples suggests the involvement of a deep calc-alkaline magmatic reservoir. Microthermometric results from Tom indicate the presence of low (120-130°C) and intermediate (170-235°C) temperature fluids; only one salinity measurement was obtained from the intermediate temperature fluid, which yielded a value of 7.9 wt.% NaCl. $\delta^{34}S$ (VCDT) values have a broad range from -12.6‰ to 20.5‰, and two sphalerite-galena pairs suggest equilibrium fractionation may have occurred between 366-388°C; $\delta^{13}C$ (V-PDB) have a restricted range from -0.5‰ to -8.6‰, apart from two groups of outliers that are either highly negative (-20‰ and -12.4‰) or highly positive (13.3‰ and 14.3‰); $\delta^{18}O$ (V-SMOW) range between 13.6‰ to 20.5‰.

INTRODUCTION

Macmillan Pass, Yukon Territory (map sheet 105 O/1, Abbott, 2013) is the location of important sediment-hosted Zn-Pb-(Ba) mineralization, including the mineral showings of Jason, Tom and Nidd. The Macmillan Pass district is situated adjacent to the NWT border, approximately 390 km NE of Whitehorse (63°1'N, 30°21'W) (**Figure 1**). Mineralization is hosted within Upper Devonian Selwyn Basin strata, specifically, a package of siliceous shales, mudstones and siltstones, and coarser-grained siliciclastic rocks, defined as the Earn Group (see Gordey *et al*., 1982). All localities display a zone of hydrothermal upflow, i.e. a cross-cutting hydrothermal vent, which forms a key genetic feature beneath the stratabound mineralization at Tom and Jason. This mineralization has previously been described as type-characteristic sedimentary-exhalative hydrothermal activity (SEDEX; Goodfellow *et al.*, 1993; Goodfellow and Lydon, 2007). Although SEDEX deposits are reported elsewhere in the geological record it is rare to find vent complexes that are as well preserved as those at Macmillan Pass. These localities therefore offer the opportunity to fully characterize the mineralogical relationships and attempt to reconstruct the bulk composition of the hydrothermal fluid. This report presents the results of detailed petrography, mineralogy, initial fluid inclusion and stable isotope analysis of vent complexes from the three localities of sediment-hosted base-metal mineralization at Macmillan Pass (Tom, Jason, and Nidd).

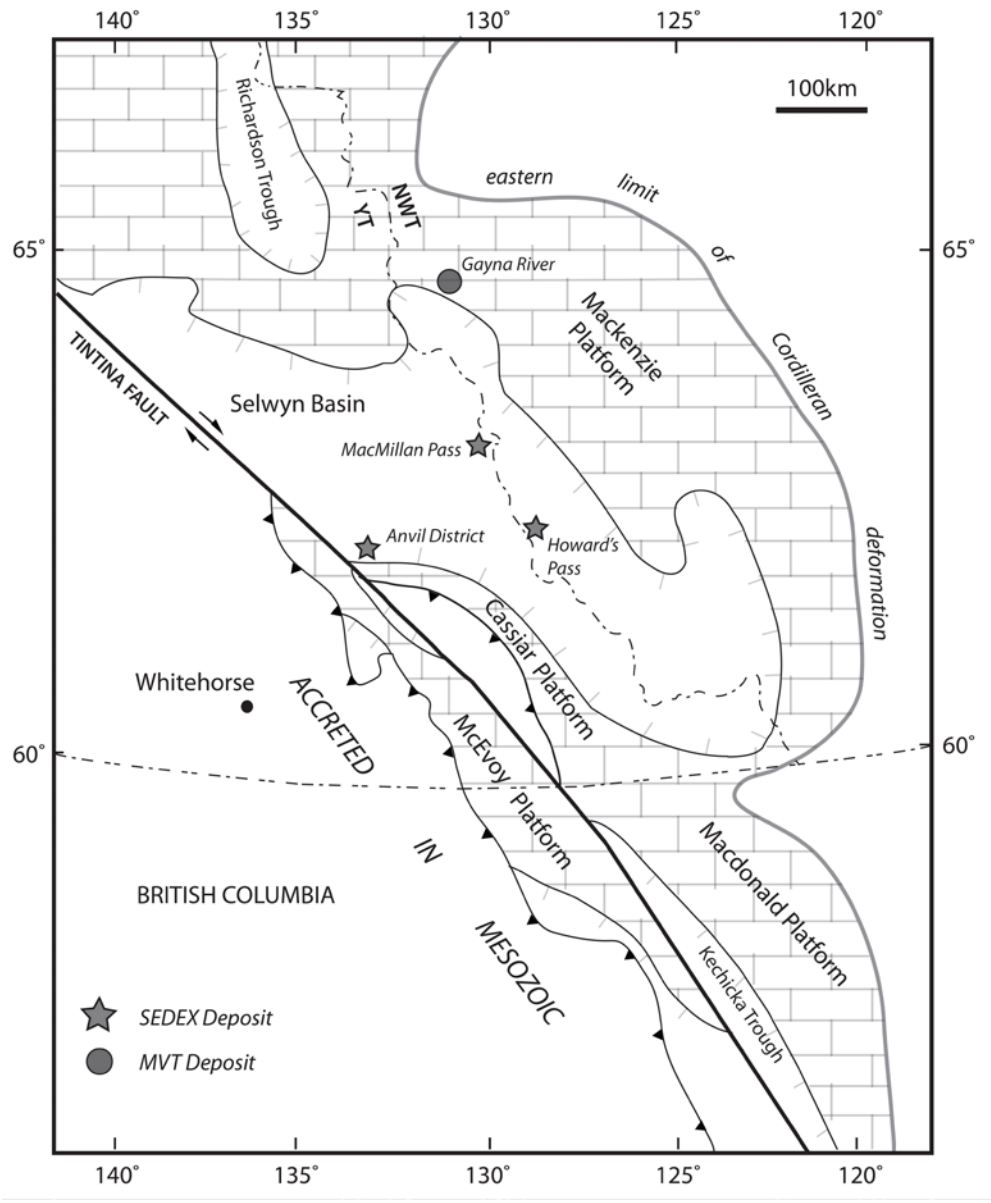

Figure 1. Map showing the geographical extent of the Selwyn Basin in the Western North America and location of the Macmillan Pass district. Modified from Gordey and Anderson (1993), Goodfellow (2007), and Nelson and Colpron (2007).

REGIONAL GEOLOGY

The Selwyn Basin was originally defined by Gabrielse (1967) as a thick, westward thickening wedge of strata of Precambrian to Middle Devonian age, deposited along the western margin of ancestral North America. The onset of basinal sedimentation was initiated by rifting associated with the continental breakup of Rodinia (~760 Ma), leading to passive margin sedimentation and forming what has traditionally been referred to as the Cordilleran *miogeocline* (Eisbacher, 1985; Gordey and

Anderson, 1993; Goodfellow *et al.,* 1995; Dickinson, 2004). The basin is now defined in terms of deep-water off-shelf sedimentation of late Precambrian to Upper Devonian age, with rift clastics forming basal and overlying strata from the late Precambrian and Late Devonian, respectively (Gordey and Anderson, 1993). Rocks of the Windermere Supergroup are the oldest exposed rocks in the Selwyn Basin, comprising a 4-6 km sequence of Neoproterozoic clastic sedimentary rocks deposited following the erosion of the crystalline basement during continental breakup (Eisbacher, 1985).

During late Devonian-Mississippian time, thick accumulations of coarse clastic sediments were deposited over the basinal strata of the Selwyn Basin. Regionally, this marked a change from an Atlantic-style passive margin to a West Pacific style convergent margin, as the western margin of ancestral North America collided with an island arc and extensional tectonics were re-activated as rifting was generated by subduction slab roll back in a distant back-arc setting (Nelson *et al.,* 2002; Lund, 2008). This tectonic setting formed the backdrop to an important period of volcanogenic massive sulphide (VMS) metallogenesis within allochthonous pericratonic terranes in the immediate arc and intra-arc settings; and more distant back-arc settings formed the proposed environment of SEDEX mineralization (Nelson and Colpron, 2007; Goodfellow, 2007).

Three episodes of magmatic activity have been identified during passive margin sedimentation, with mafic volcanic flows, dykes and tuffs observed in Early Cambrian, Middle Ordovician, and Middle to Late Devonian strata (Goodfellow, 2007). The observation of alkalic and ultrapotassic volcanic rocks associated with syn-rift clastic rocks during the lower to middle Paleozoic has been used as evidence for widespread extensional tectonics; the incompatible element chemistry of these units suggests an origin similar to that observed in alkaline basalts formed in continental rifts (Goodfellow *et al.,* 1995). Intrusive rocks of mid-Cretaceous to Tertiary (124-62 Ma) age form the final component of Selwyn Basin regional geology. They were emplaced into the deformed continental strata produced during Mesozoic island arc accretion to the margin, and they provide an important setting for intrusion related deposits (Hart *et al.,* 2004; Thiessen *et al.,* 2012).

As a result of deformation related to Mesozoic island arc accretion, the passive margin strata have been incorporated into the northern Cordillera fold and thrust belt. Basinal strata form the *inner belt*, characterised by regional-scale folds and thrusts and accompanied by slaty cleavage and intense tight to isoclinal folding; platformal carbonates form the *outer belt* and represent the eastern most extent of deformation (Gordey *et al.,* 2010). The final age of deformation is late Early Cretaceous, as determined by crosscutting of strata by mid-Cretaceous plutonic rocks (Gordey *et al.,* 2010).

LOCAL GEOLOGY

The Zn-Pb-(Ba) sediment-hosted mineralization at Tom, Nidd and Jason are hosted in the Earn Group, which contains the Portrait Lake Formation (Lower Earn Group) and the Prevost Formation (Upper Earn Group) (**Figure 2**). The main phase of stratabound mineralization was localized within the Portrait Lake Formation, specifically within the Macmillan Pass Member (Abbott and Turner, 1990). This member contains pebble conglomerate, diamictite interbedded with sand and shale, and silt laminated mudstone (Abbott and Turner, 1990; Magnall and Gleeson, 2012a). Variability in bed thickness of the coarse clastics in the local area of Macmillan Pass has been interpreted to represent the existence of a number of basin-bounding faults and sedimentation in a syn-tectonic environment (Abbott and Turner, 1990).

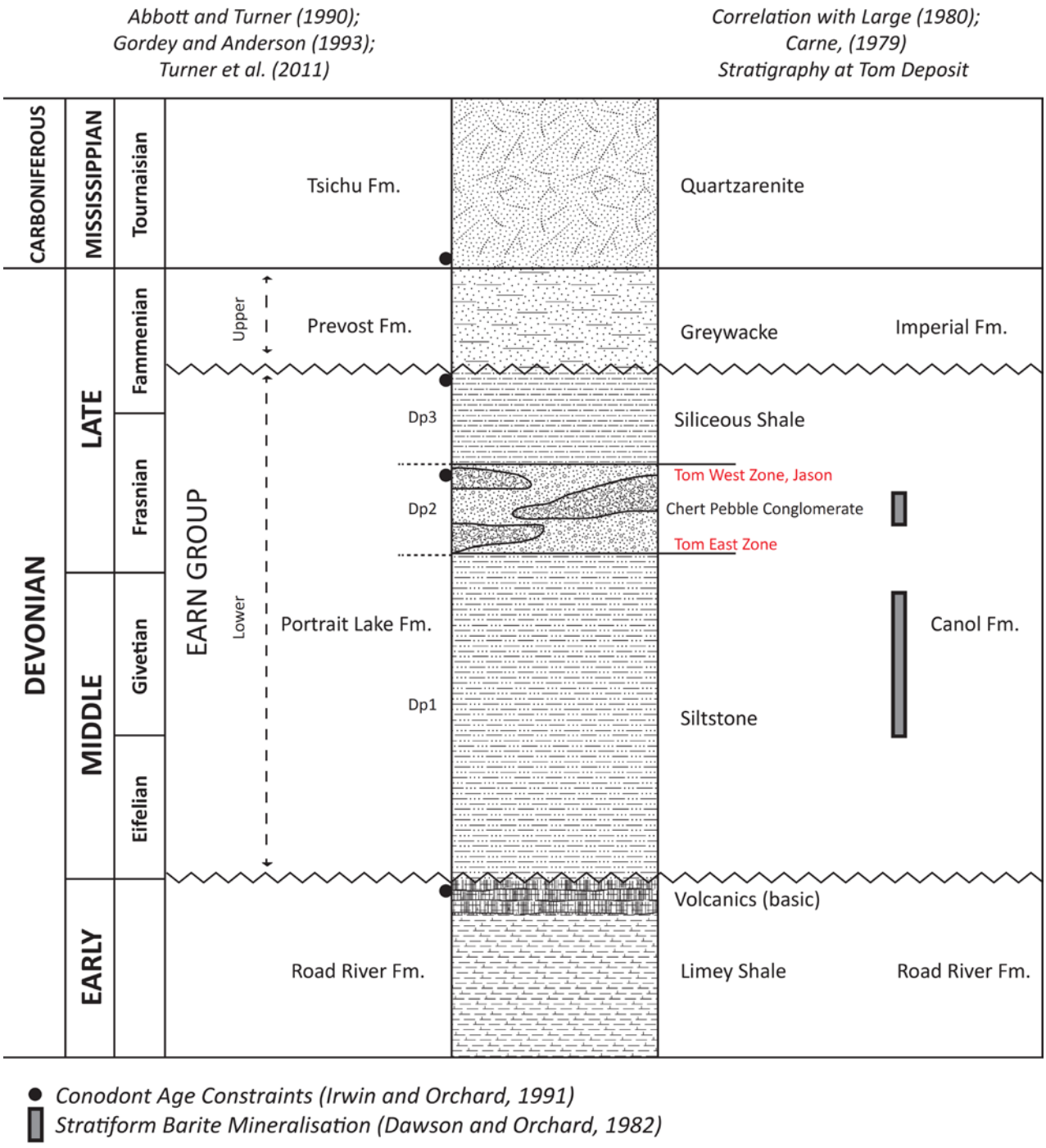

Figure 2. The stratigraphy of Late Devonian strata at Macmillan Pass. Figure compiled from Carne (1979), Large (1980), Dawson and Orchard (1982), Abbott and Turner (1990), Irwin and Orchard (1991), Gordey and Anderson (1993), Turner *et al.* (2011).

The host rock to the Tom (West Zone) and Jason deposits has been dated as mid-Frasnian by conodont biostratigraphy (Irwin and Orchard, 1991). Mineralization at Macmillan Pass has previously been considered syn-sedimentary, and so this biostratigraphic marker has been used to constrain the timing of hydrothermal mineralization (Goodfellow *et al.*, 1993; Goodfellow and Lydon, 2007). Macmillan Pass also hosts stratabound barite deposits within the same stratigraphic horizon as base metal deposits, potentially representing the distal expression of the hydrothermal activity that produced Tom and Jason (Goodfellow and Lydon, 2007; Fernandes, 2011). Fifteen km west of Jason, the epigenetic Pb-Zn sulphide minerals at Boundary Creek (Nidd) are similar to those at Tom and Jason, and are also hosted by the Macmillan Pass Member (Turner and Rhodes, 1991; Magnall and Gleeson, 2012b). As no stratabound sulphide minerals are observed at Nidd (only vent complex), it is possible that this occurrence represents either a failed feeder zone or that the overlying stratabound facies was not preserved.

Tom, Jason and Nidd are located within the central block of the Macmillan Fold Belt (MFB), formed during Mesozoic deformation and characterized by west-trending folds that contrast with the more northwest regional trend (Abbott, 1982). Structures are clearly Mesozoic in age, but the differences in style between the blocks of the MFB indicate that deformation may be influenced by pre-existing Devonian structures (Abbott, 1982; Abbott and Turner, 1990).

ANALYTICAL TECHNIQUES AND DATA COLLECTION

Petrography

Samples from Nidd and Tom were collected during the respective 2010 and 2012 field seasons, from core storage at Macmillan Pass (Tom camp). The sampling of Jason drill-core was performed during the 2013 field season from core storage near the Macmillan Pass airstrip. Samples from the vent complexes were targeted, along with under- and overlying strata. Hand samples have been described and ~160 thin sections made for detailed optical microscopy under reflected and transmitted light. A desktop cold cathode-tube cathodoluminscence microscope (University of Alberta) was used to examine compositional and textural relationships between different generations of quartz at Nidd. The samples from Tom and Nidd have been described in detail in Magnall *et al*. (2014).

Fluid Inclusion Analysis

Doubly polished, 70-100μm thick fluid inclusion wafers (n=30) were prepared by Vancouver Petrographics and analysed under transmitted and reflected light to determine paragenetic relationships. Minerals in equilibrium and / or displayed close paragenetic relationships with sulphide phases were targeted for fluid inclusion analysis. These fluid inclusions were then classified as secondary, pseudo-secondary or primary according to the criteria defined by Roedder (1984). They are described according to the phases present at room temperature (L_W = liquid water, L_C = liquid CO_2, V = vapour). Microthermometry was performed using a Linkham THMSG600 heating/freezing stage that has a working range of -196 to 600°C. The stage was calibrated at -56.6°C, 0°C and 374.1°C using SynFlinc synthetic standards, with accuracy ±0.2°C. Salinity measurements (NaCl wt.%) were calculated using the equation of Bodnar (1993). Quantitative fluid inclusion gas analysis was performed using the incremental crush fast scan method described by Blamey (2012).

Stable Isotopes

Carbon and oxygen isotope analyses were performed at Isotope Science Laboratory (University of Calgary). Samples were hand picked from disaggregated core samples under the binocular microscope. Attempts were made to pick mineral phases that were in textural equilibrium to enable calculation of equilibrium temperatures. Mineral separates were ground to <50μm using an agate mortar and pestle. Samples were then digested with anhydrous phosphoric acid in a reaction vessel at 25°C to produce CO_2 introduced to the ion source of a VG 903, stable isotope ratio mass spectrometer. Analyses of $^{13}C/^{12}C$ and $^{18}O/^{16}O$ ratios are reported in the per-mille notation relative to the international Vienna Pee Dee Belemnite (V-PDB) and Vienna Standard Mean Ocean Water (V-SMOW) standards, with precision and reproducibility typically better than ±0.2‰.

As with samples for carbon and oxygen, sulphide separates were obtained from disaggregated core samples under the binocular microscope. Samples were introduced to a quartz tube combustion reactor (T = 1050°C), and eluent gases transferred by a helium carrier stream through a gas chromotograph to achieve gas separation before subsequent mass spectrometry (see method of Grassineau *et al.*, 2001). Analysis of the $^{34}S/^{32}S$ ratio is reported in the per-mille notation relative to the Vienna-Canyon Diablo Troilite standard (V-CDT), with precision and reproducibility typically better than ±0.3‰.

RESULTS

Mineralogy and Petrography

The hydrothermal vents at Tom, Nidd and Jason are all hosted within a radiolarian-bearing, siliceous mudstone. The mineralogy, alteration and petrography of samples from Tom and Nidd have already been described in detail in earlier publications (Magnall and Gleeson, 2012a, b; Magnall *et al*., 2014). To summarise, both display stock-work style hydrothermal veining. Distinctive, orange weathering Fe-carbonate veins and intense alteration is most characteristic at Tom, whereas at Nidd the vent is more host-rock dominated, with discrete veining and less intense alteration. The following section describes the vent at Jason (**Figure 3**), which is more typical of the style of mineralization described at Tom than at Nidd.

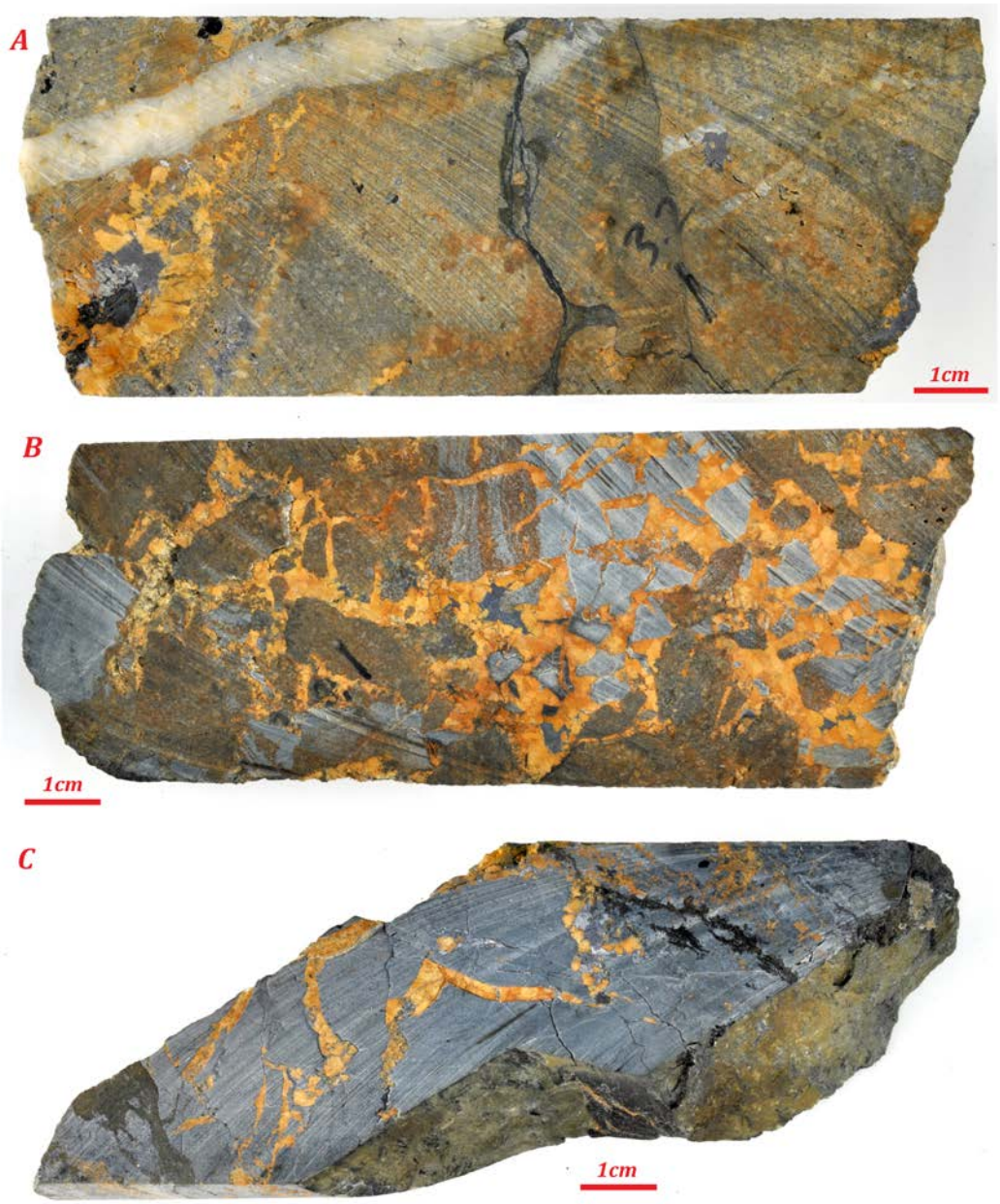

Figure 3. Samples from the vent at Jason. A – intense carbonate alteration and massive sulphide replacement of host-rock. Sample also displays vuggy ankerite veining with space-filling galena in the lower left corner (DH 82-86A, 710m). B – stock-work style ankerite veining with space-filling vuggy galena. Host rock displays inter-clast variability in carbonate alteration and massive sulphide replacement (DH 82-86A, 719m). C – sample from the margin of the vent where alteration of the host rock is much less extensive (DH 82-86A, 729m).

Jason - Stage 1

As with Tom, an assemblage of pyrite, ankerite and quartz typify the hydrothermal veining in the vent at Jason (*Stage 1*): Pyrite occurs in a variety of forms; massive (>1cm) anhedral aggregates are most common, and they are intergrown with smaller (<500µm) interlocking subhedral ankerite crystals

(**Figure 4A**). Smaller subhedral crystals occur within quartz-ankerite veins, along with minor magnetite (**Figure 4B**). Multiple generations of this assemblage are observed, with small veinlets of ankerite and quartz often crosscutting each other.

Jason - Stage 2

The deposition of base metals is clearly constrained within *Stage 2*, in a simple assemblage of galena, pyrrhotite, chalcopyrite, pyrite and sphalerite. *Stage 2* pyrite (Py-2) is clearly observed crosscutting *Stage 1* pyrite (Py-1) (**Figure 4A**), and also appears within veinlets of galena, pyrrhotite and chalcopyrite, all of which crosscut earlier stage 1 mineralization (**Figure 4C**). Sphalerite is only a minor component of the vent at Jason, and is only occasionally found with galena and associated more intimately with chalcopyrite in veins crosscutting *Stage 1* (**Figure 4D**). Base metals also occur as massive sulphide replacement of *Stage 1*, with galena and pyrrhotite forming widespread, fine-grained anhedral replacement of ankerite and pyrite (**Figure 4E** and **F**).

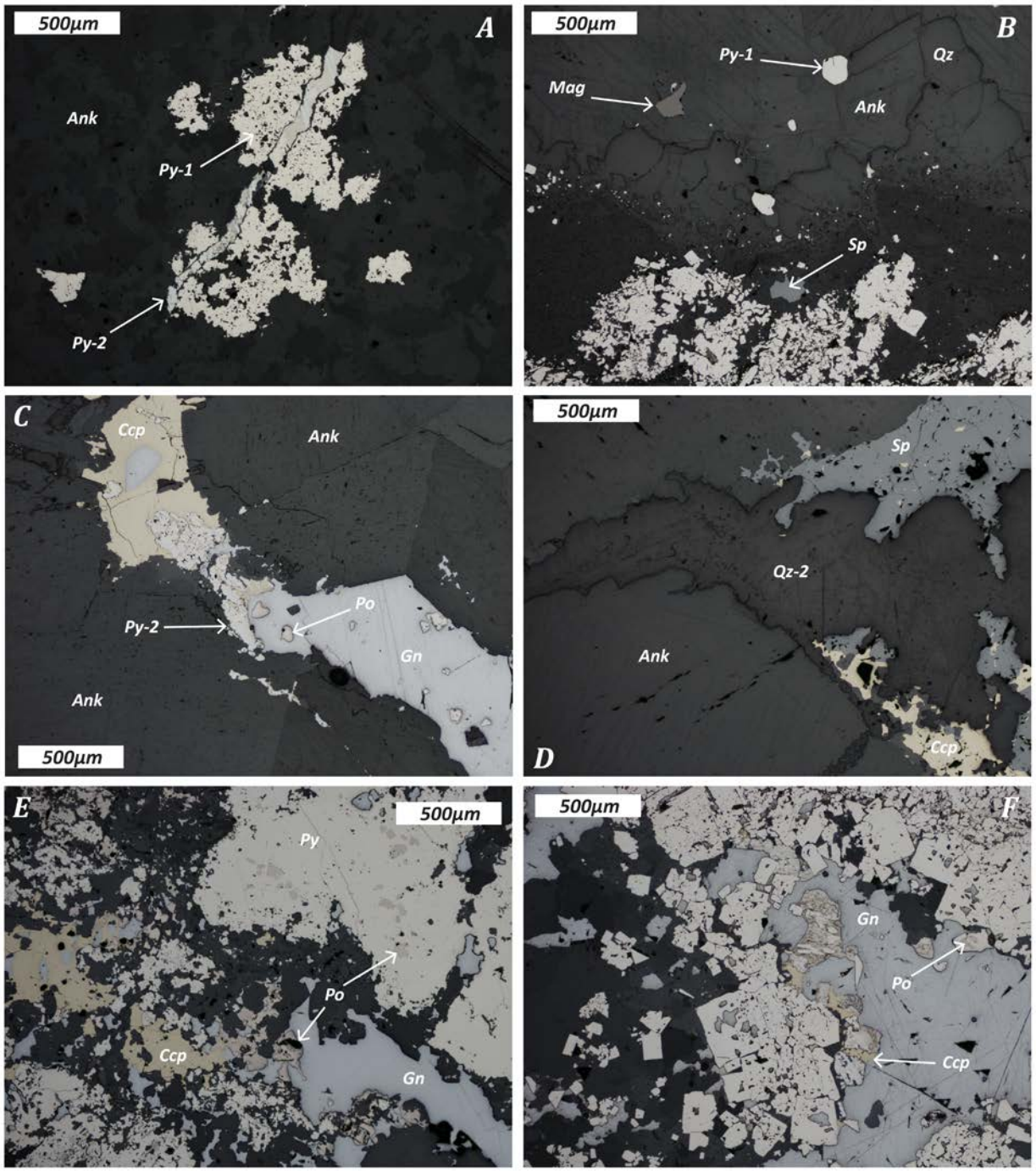

Figure 4. Reflected light photomicrographs from the vent at Jason. A – aggregate of early anhedral pyrite (Py-1) intergrown with ankerite (Ank) and cut by later Stage 2 pyrite (Py-2). B – vein growth from pyritized mudstone wall-rock. Vein mineralogy is quartz (Qz) followed by ankerite with minor pyrite (Py-1) and magnetite (Mag). C – Stage 2 sulphide mineral assemblage of galena (Gn), chalcopyrite (Ccp), pyrrhotite (Po) and pyrite (Py-2) within veinlet crosscutting earlier Stage 1 ankerite. D – Stage 2 veinlet containing quartz (Qz-2) associated with sphalerite (Sp) and chalcopyrite crosscutting earlier Stage 1 ankerite. E – massive sulphide replacement of earlier carbonate and pyrite altered host-rock. Widespread replacement by galena, chalcopyrite and pyrrhotite. F – as with E, massive sulphide replacement of pyrite by galena and minor chalcopyrite and pyrrhotite.

A summary paragenetic sequence for Tom, Nidd and Jason is presented in **Figure 5**. In order of relative abundance, sulphides include pyrite and galena, pyrrhotite, sphalerite, chalcopyrite, magnetite, arsenopyrite and minor sulphosalts (tetrahedrite and bournonite). For Tom and Jason, some vent material is highly enriched in sulphides, with samples comprising of >30% galena ± pyrite ± (sphalerite, pyrrhotite, chalcopyrite).

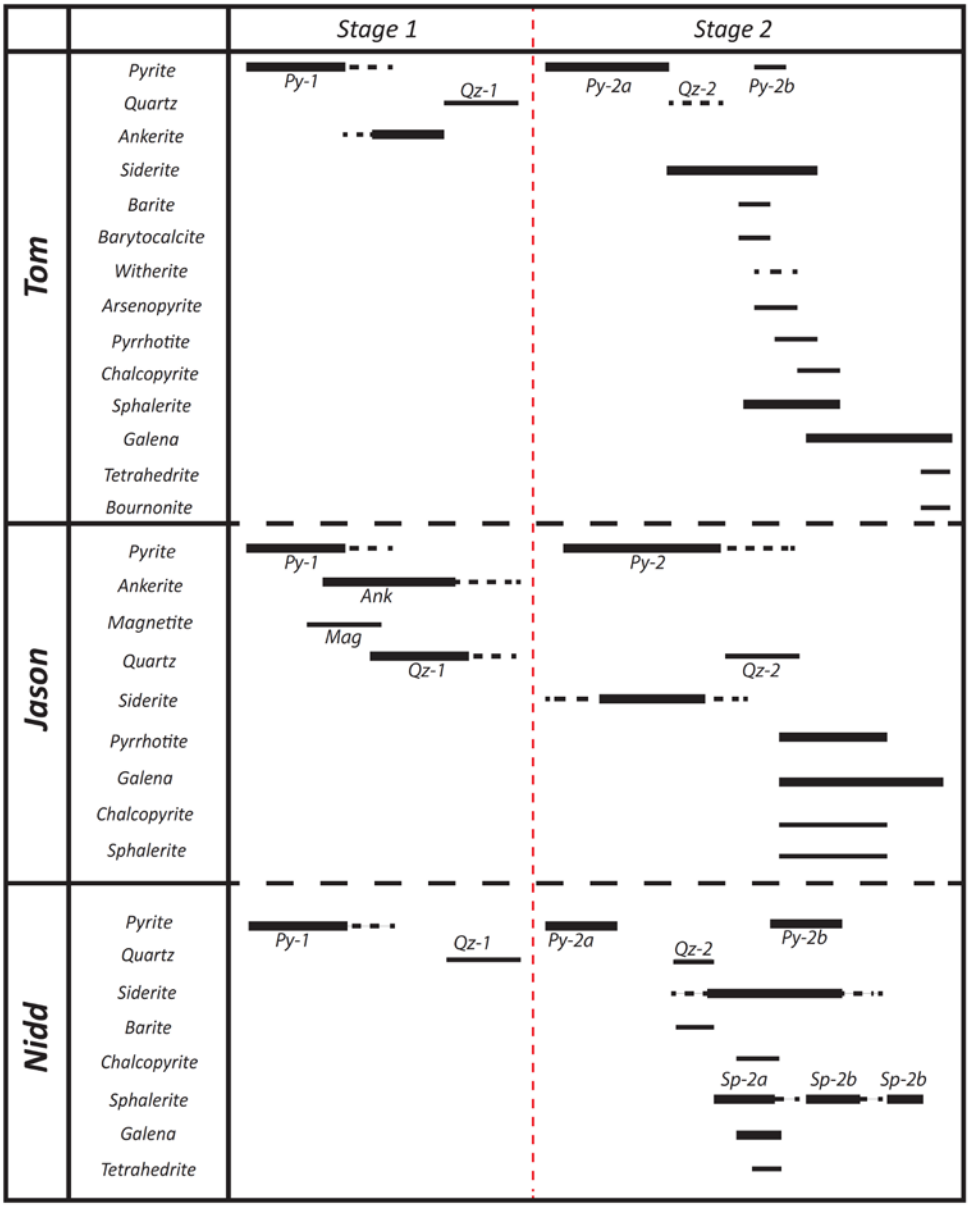

Figure 5. Mineral paragenesis for the vent complexes at Tom, Jason and Nidd. All three display two clear stages of mineralization. Stage 1 is characterized by iron carbonate, pyrite and quartz, with minor magnetite at Jason. The deposition of ore-forming base-metal sulphides occurs with Stage 2.

Alteration

Iron carbonate and pyrite are the dominant minerals in the alteration assemblage that characterize the vent complex at Jason. This alteration assemblage is also observed in the vent complex at Tom, and as a halo around the vent in the sediments surrounding mineralization at both localities. Alteration is associated with *Stage 1* of the paragenesis, and occurs predominantly as small, interlocking euhedral ankerite crystals and massive anhedral aggregates of pyrite that destructively overprints the host rock. Stock-work style veins that display the same mineralogy then crosscut this alteration. This repetition of ankerite, albeit in different styles, likely represents the telescoping of the system and provides evidence for multiple pulses of the hydrothermal fluid.

Fluid Inclusion Petrography

From the paragenetic sequence presented in **Figure 5**, it is clear that there are limited mineral phases (siderite, barite, barytocalcite and quartz) that are associated with the principal ore forming components, galena and sphalerite. There are abundant inclusions within Stage 1 minerals (quartz and ankerite), however they are mostly either too small for analysis (<5µm), or cannot be demonstrated to be of primary origin.

Nidd: Detailed desktop CL petrography was used to determine the paragenetic context of quartz at Nidd. The results indicate that two quartz generations are present within the paragenesis, but only the latter (Qz-2 Stage 2) is associated with sphalerite. Quartz-2 contains a dominant inclusion assemblage of 3-phase aqueous-rich CO_2 (L_w + L_c + V), 2 phase aqueous-poor CO_2 (L_c + V) and single-phase (V) inclusions (**Figure 6**). Inclusions are generally no larger than 15µm, and mostly <10µm. Quartz-I also contains similar inclusions, however this earlier generation of quartz is typically fractured and it is not possible to determine whether inclusions are primary.

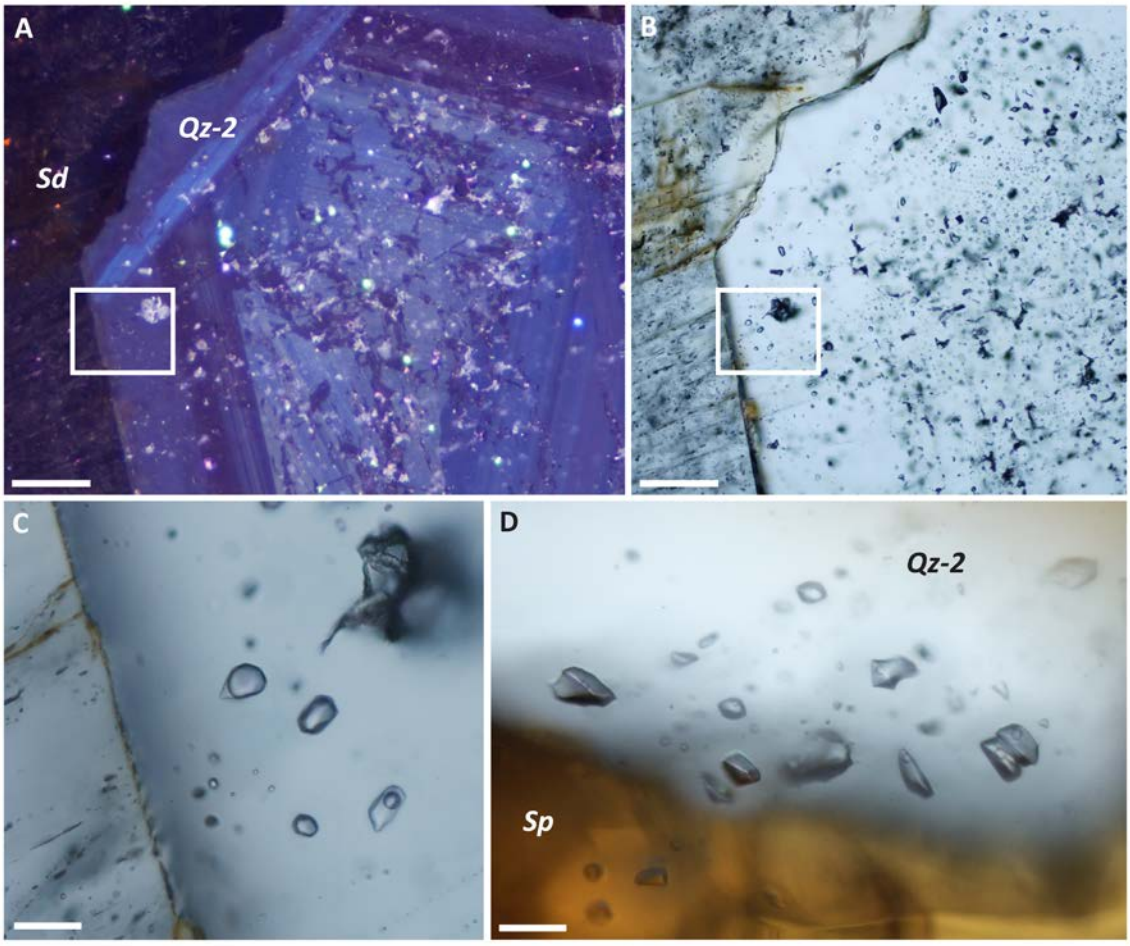

Figure 6. A – desktop-CL image of Qz-2, showing clear growth zonation. Box highlights the area containing a primary fluid inclusion assemblage (see C). Scale bar = 100µm. B – transmitted light image of image A. Scale bar = 100µm. C – transmitted light image of area highlighted in A and B displaying the primary fluid inclusion assemblage. Scale bar = 20µm. D – 2 phase carbonic inclusions in Qz-2 intimately associated with sphalerite. Scale bar = 20µm. Abbreviations: Sd – siderite, Qz-2 – quartz, Sp – sphalerite.

Tom: Primary inclusions have been identified in barite, barytocalcite and siderite and quartz. These mineral phases are not volumetrically significant within the vent complex, however they are clearly associated with base metal mineralization (**Figure 7**). They contain small (~10µm), randomly distributed and irregular two-phase (L_w + V) inclusions, which although do not form along growth zones, pre-date minor fractures and are the likeliest candidate for primary inclusions. A CO_2-bearing assemblage is also present, both in Stage 1 and Stage 2, and although it bears resemblance to the CO_2-bearing inclusions from Nidd, further work needs to be carried out to confirm a primary origin.

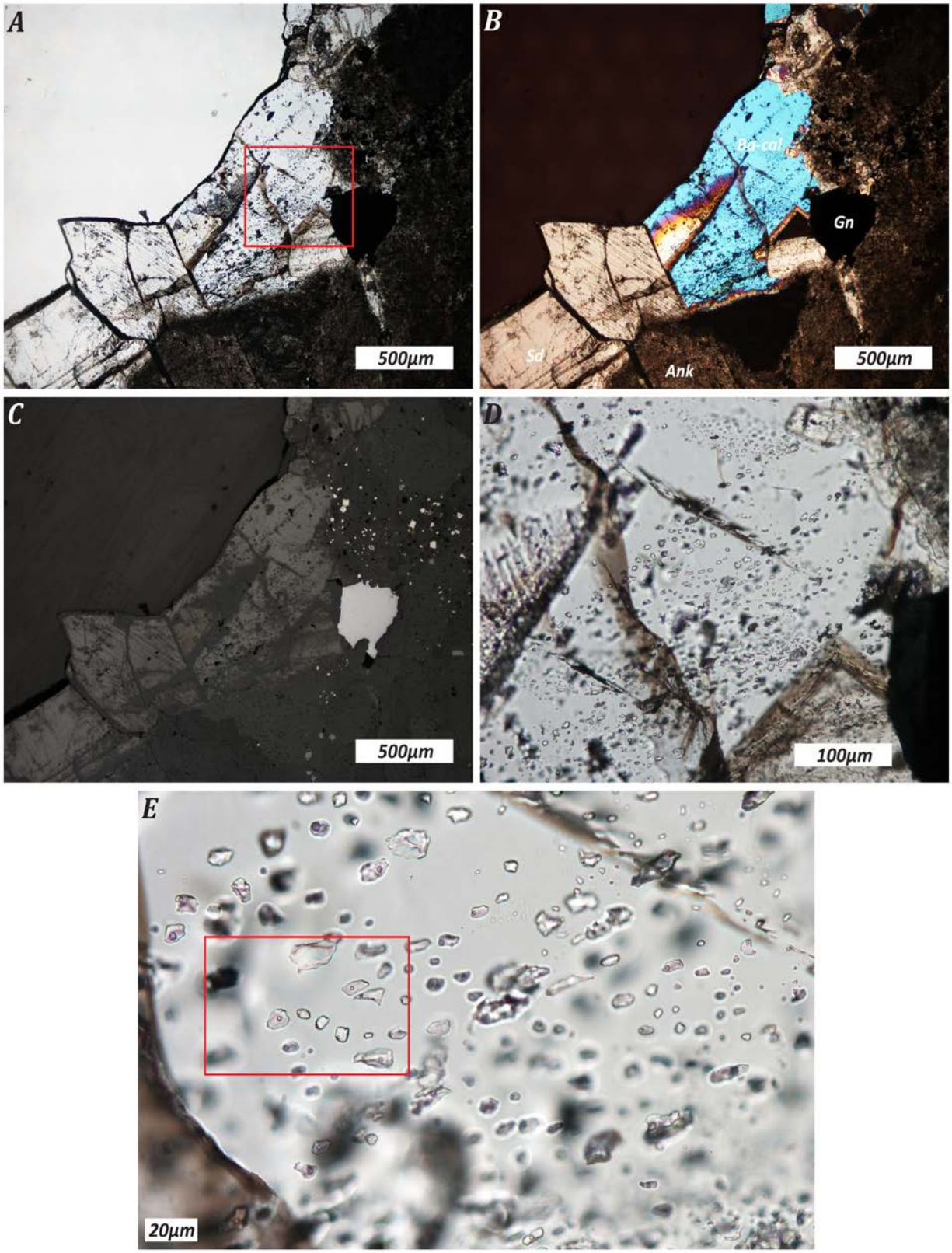

Figure 7. A – transmitted light image of sulphide-bearing Stage 2 veinlet from vent at Tom (DH TU71-4). B – cross polarized image of A, clearly displaying the gangue mineralogy. C – reflected light image. D – close up of area highlighted in A. E – primary 2 phase (Lw + V) fluid inclusion assemblage. Abbreviations: Ba-cal – barytocalcite, Gn – galena, Sd – siderite, Ank –ankerite.

Fluid Inclusion Microthermometry

The initial results of microthermometry on inclusions from Nidd and Tom are presented in **Table 1** (Nidd) and **Table 2** (Tom). The inclusions at Nidd contain pure CO_2, and although some clathrate melting temperatures were obtained, they should be treated with caution due to the difficulty in observing this phase transition in such small inclusions. The initial results from a sample at Tom displays two groups of data; there is a relatively low temperature assemblage (120-130°C; n = 9) for which it was not possible to view low temperature phase transitions, and a broader, more intermediate temperature assemblage (170-234°C; n = 12) for which one low temperature salinity measurement was possible (NaCl wt.% = 7.9).

Table 1. Microthermometric results from Nidd. Melting of solid CO_2 is reported as T_mCO_2, melting of clathrate as T_mCLATH, and homogenization of CO_2 as T_HCO_2.

Sample	CHIP	Section	Inclusion #	T_mCO_2 (°C)	T_mICE (°C)	T_mCLATH (°C)	T_HCO_2 (°C)
349.1	1	A	1	-57.7		9	25
349.3	1	A	1	57.1		9	13.8
			2	57.1			15.6
			3	57.1			26
			4	57.1		9	28
			5				13.8
			6				13
			7				15
			8				16
			9				17.6
		B	1				16
			2				15
			3			9	30.7
			4				29.3
349.4	1	A	1	-56.6		9	18
			2	-56.6		9	14
			3	-56.6		9	18
	3	A	1	-56.7			24.8
			2	-56.7			24.8
			3	-56.7			24.8
			4	-56.7			25
			5	-56.7			24
			6	-56.7			24
			7	-56.7			24
			8	-56.7			24
			9	-56.7			25
			10	-56.7			25
			11	-56.7			25
			12	-56.7			24.5
	3	B	1	-56.7			
			2	-56.7		8.5	
			3	-56.7		8.5	
			4	-56.7			
			5	-56.7			
			6	-56.7			
			7	-56.7			
			8	-56.7			
	3	C	1	-56.7		9	25
			2	-56.7		9	25
			3	-56.7		9	25
349.8	1	A	1	-56.8		8	31.1
			2	-56.8		0	8
		B	1	-56.7		8.5	26
			2	-56.7		8.5	25
	4	A	1	-56.6		-26.5	11
			2	-56.6		6.5	11

Table 2. Microthermometric results from Tom. Final melting of ice is reported as T_mICE, and respective homogenization and description temperatures as T_H and $T\text{-}_d$. Degree of filling is indicated in the final two columns as the proportion of liquid or vapour in each inclusion.

Sample	CHIP	Section	Inclusion #	T_mICE	T_H (°C)	$T\text{-}_d$ (°C)	NaCl wt. %	Liquid	Vapour
TU71-4	1	A	1		120			0.95	0.05
			2		126			0.95	0.05
			3		120			0.95	0.05
			4		120			0.95	0.05
			5		120			0.95	0.05
			6		120			0.95	0.05
			9		120			0.95	0.05
			10		130			0.95	0.05
		B	1			200			
			4			200			
			7		136				
TU71-4	2	A	1		225			0.85	0.15
			2		170			0.85	0.15
			3		206			0.85	0.15
			4			190		0.85	0.15
		B	1		234			0.85	0.15
			2		234			0.85	0.15
			3		225			0.85	0.15
			4		226			0.85	0.15
			5		226			0.85	0.15
			6			140		0.85	0.15
						140		0.85	0.15
		D	1	-5	213		7.9	0.85	0.15

Fluid Inclusion Gas Analysis

The results of gas mass spectrometry from fluid inclusions hosted in Qz-I and Qz-II obtained from samples from the vent at Nidd are presented in **Figure 8**. Results fall within the reservoir for calc alkaline magmatic gases as defined by a compilation of fluid inclusion gas results produced by Blamey (2012).

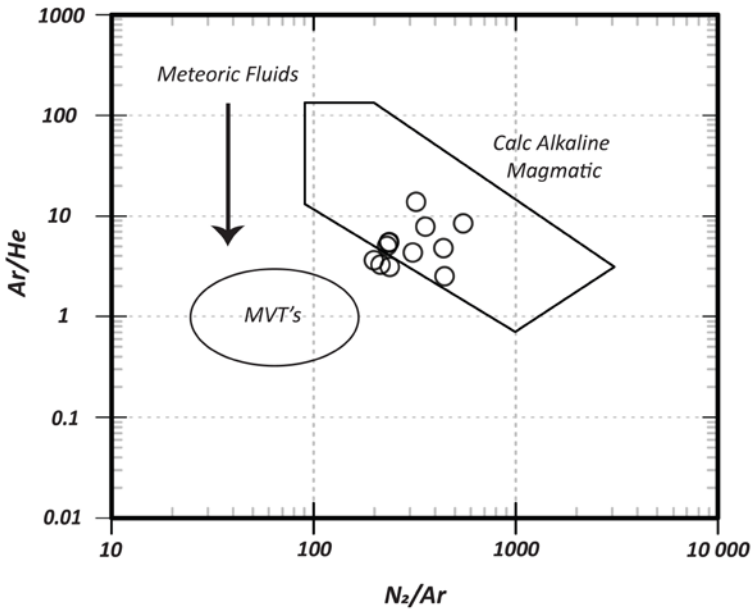

Figure 8. N_2-Ar-He compositional plot from fluid inclusion gas analysis of samples from Nidd. Plot adapted from Blamey (2012).

Sulphur, Carbon and Oxygen Isotopes

Sulphur isotope results from galena, sphalerite and pyrite display a wide range of values ranging between -12.6‰ and 20.53‰ ($\delta^{34}S$; V-CDT), with a median value of 14.3‰ (*n = 46*) (see **Figure 9**). In a handful of samples, sphalerite and galena display evidence of textural equilibrium. If isotopic equilibrium is assumed with $\Delta_{sp\text{-}gn}$ values for two samples from Jason of 1.6‰ and 1.7‰, the isotopic thermometer of Czamanske and Rye (1974) suggests an equilibrium temperature between 368 and 388°C.

Carbon and oxygen isotope results (*n = 24*) of iron carbonate in the hydrothermal vents (Tom, Jason and Nidd), surrounding alteration and overlying mineralization is presented in **Figure 10**. They display greater variation than previously documented in Ansdell *et al*. (1989) and Gardner and Hutcheon (1985). There are two groups of data; the first displays high and low $\delta^{13}C$ values ($\delta^{13}C$ = 13.3‰ to 14.3‰ and -20‰ and -12.4‰) that fall within the respective reservoirs for carbonate derived organic matter fermentation and sulphate reduction of organic matter, whereas the second group displays a narrower range ($\delta^{13}C$ = -0.5 to -8.6‰). The $\delta^{18}O$ composition for both groups ranges between 13.6 and 20.5‰.

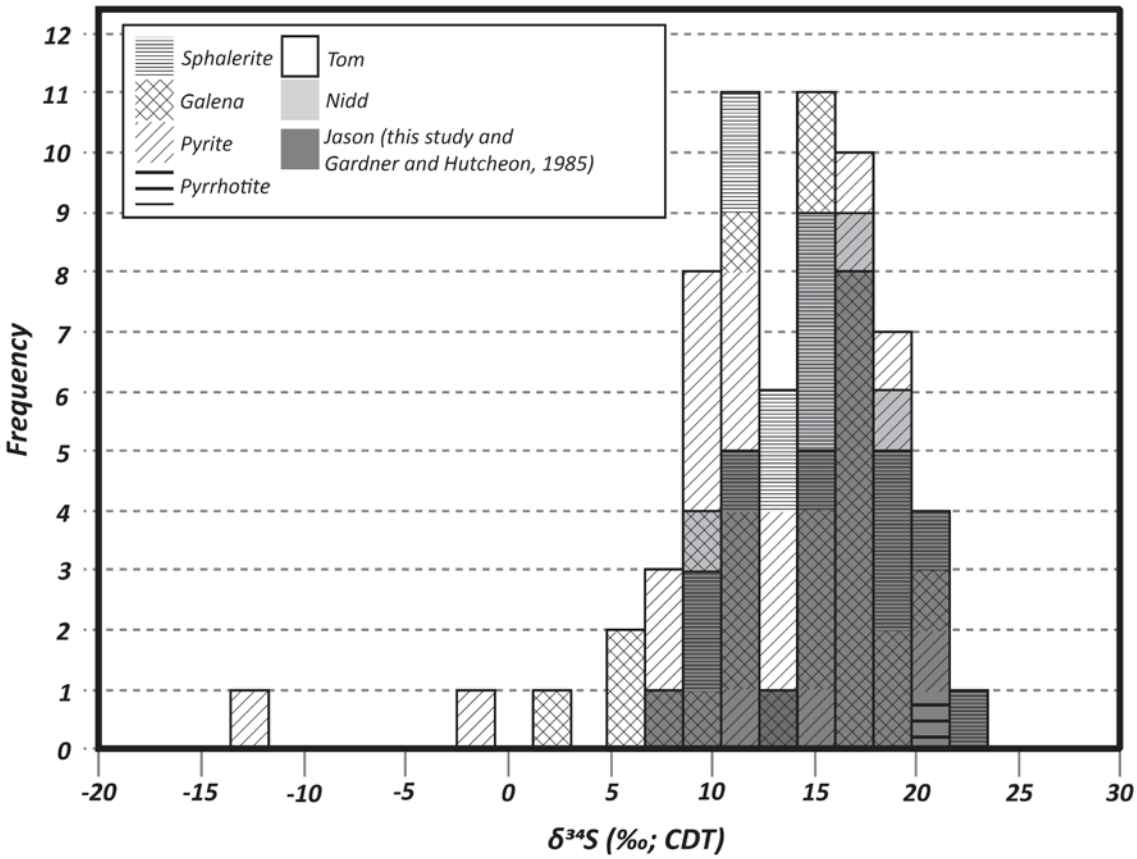

Figure 9. Frequency histogram of sulphur isotope results from Tom, Jason and Nidd. Analyses were carried out on sphalerite, galena, pyrite and one pyrrhotite sample. Data from Gardner and Hutcheon (1985) is also included.

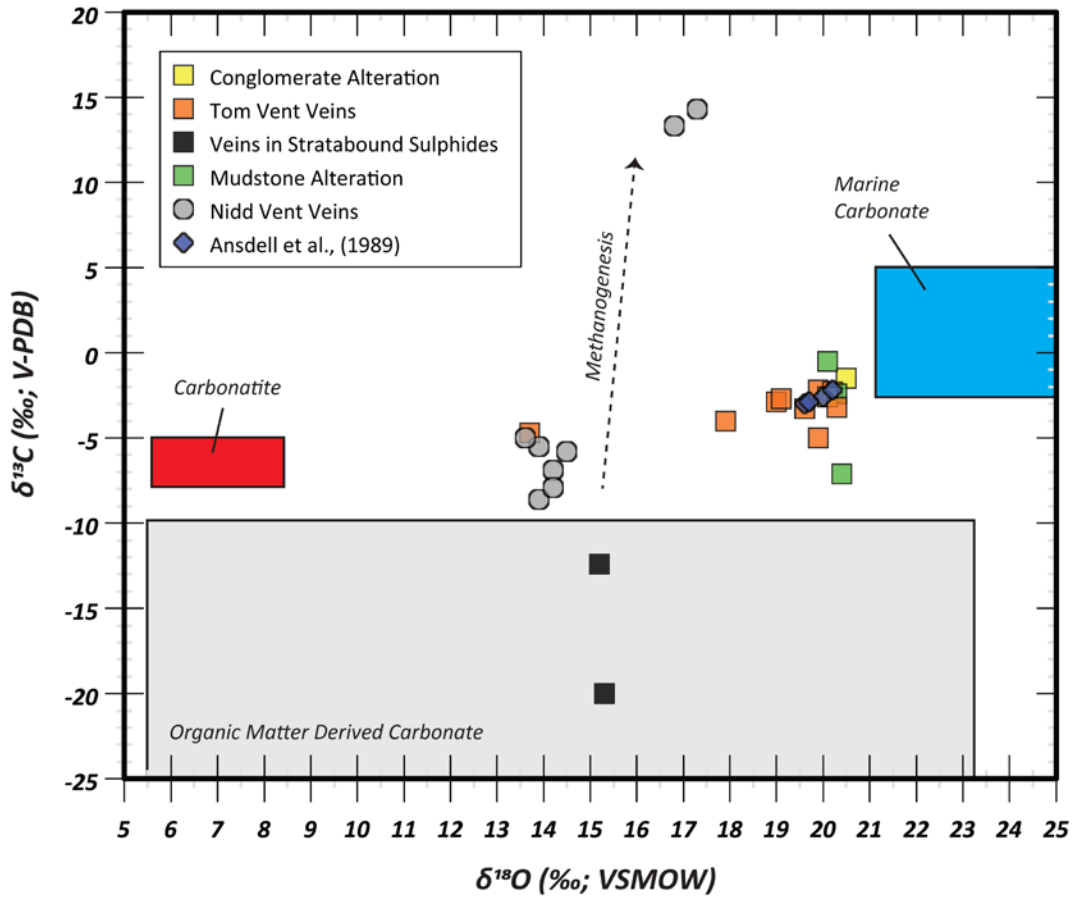

Figure 10. Oxygen vs carbon isotope plot for samples from the hydrothermal vent at Tom and Nidd, along with alteration from the vent complex and veins host in overlying stratabound sulphide mineralization. Results from Ansdell *et al*. (1989) are also included. Reservoirs are defined by Valley (1986) for carbonatite, Veizer *et al.* (1999) for Late Devonian marine carbonate, and Longstaffe (1989) for carbonate derived from breakdown of organic matter.

DISCUSSION

The initial results of detailed petrography, stable isotope and fluid inclusion analysis provide useful insight on the hydrothermal systems that operated in the Upper Devonian strata at Macmillan Pass. In the first instance, the observation that there are two distinct phases of fluid flow preserved within the hydrothermal vents enables the results of previous studies to be interpreted with more care. The majority of fluid inclusion analyses reported by Ansdell *et al*. (1989) and Gardner and Hutcheon (1985) appear to be from Stage 1 ankerite, and the wide range of temperature and salinity data (2 – 18 NaCl wt.%; T = 157 - 335°C) they report may reflect the effects of overprinting by the later Stage 2 mineralization. In addition, although CO_2 inclusions were reported in these earlier studies, a temporal context (primary vs. secondary) was not clearly indicated. At Nidd, this assemblage has been proven to be primary, and interestingly it preserves evidence of the entrapment of a heterogeneous fluid,

suggestive of phase immiscibility (i.e. fluid boiling). Gas analysis indicates this dominant fluid inclusion assemblage may have a deep origin, as the N_2-Ar-He composition suggests a calc-alkaline magmatic origin (see **Figure 8**) (Blamey, 2012).

Evidence of deep, hot processes are preserved in the form of highly positive Eu/Eu* anomalies, reported from the vents of Tom and Nidd (Magnall *et al*., 2013). These suggest fluid temperatures exceeded 250°C, a conclusion supported by the temperatures calculated using S isotope pairs from sphalerite and galena. However, such high inferred temperatures may also indicate that sphalerite and galena did not reach isotopic equilibrium. Evidence of mixing with a cooler, shallow fluid is shown by the low-temperature fluid inclusion assemblage preserved at Tom, and also the negative Ce/Ce* anomalies preserved in the same vent samples (Tom and Nidd), which indicate an oxidizing seawater component.

The contribution of shallow, diagenetic processes to the hydrothermal system is preserved in the carbon and sulphur isotopic composition of gangue minerals in the vent complexes. Highly negative $\delta^{13}C$ values in carbonate veins overlying the vent indicate carbonate derived from organic matter degradation, whereas highly positive values suggest organic fermentation at greater depths. The negative $\delta^{34}S$ values preserved in pyrite indicate that there is a minor volumetric contribution of reduced sulphur from bacterial sulphate reduction.

CONCLUSION

Detailed petrography indicates that base metal sulphides were deposited following an initial stage of widespread stock-work style ankerite and quartz veining at both Tom and Jason. The input of volatiles and heat from deep within the fluid systems at Macmillan Pass is indicated in the gas analysis at Nidd, equilibrium fractionation between sphalerite and galena and a high temperature fluid inclusion assemblage (Tom). Initial fluid inclusion analysis that has targeted volumetrically minor phases, intimately associated with the base metal sulphides, indicates the possible role of fluid mixing in the deposition of metals from the hydrothermal fluid. Future work will target similar phases for fluid inclusion analysis within the vent at Jason, which displays similar paragenetic relationships as those observed at Tom.

ACKNOWLEDGMENTS

This project was funded by the Targeted Geoscience Initiative program of the Geological Survey of Canada. We are grateful to Keith Dewing of the Geological Survey of Canada in Calgary for his excellent review of the manuscript.

REFERENCES

Abbott, J.G., 2013. Bedrock geology of the Macmillan Pass area Yukon and adjacent Northwest Territories (NTS 105O/1, 2 and parts of 105O/7, 8 and 105P/4, 5) (1:50,000 scale); Yukon Geological Survey Geoscience Map 2013-1.

Abbott, J.G., 1982. Structure and stratigraphy of the Macmillan Fold Belt; evidence for Devonian faulting; *in* Yukon Geology and Exploration-1981; Exploration and Geological Services Division, Yukon, Indian and Northern Affairs Canada, p. 22-33.

Abbott, J.G. and Turner, R.J., 1991. Character and paleotectonic setting of Devonian stratiform sediment-hosted Zn, Pb, Ba deposits, Macmillan Fold Belt, Yukon; *in* Mineral Deposits of the Northern Canadian Cordillera, Yukon - Northeastern British Columbia [Field Trip 14], (ed.) Abbott, J.G. and Turner R.J.W.; Geological Survey of Canada, Open File 2169, p. 99-136.

Ansdell, K.M., Nesbitt, B.E., and Longstaffe, F.J., 1989. A fluid inclusion and stable-isotope study of the Tom Ba-Pb-Zn deposit, Yukon Territory, Canada; Economic Geology, v. 84, p. 841-856.

Blamey, N.J.F., 2012. Composition and evolution of crustal, geothermal and hydrothermal fluids interpreted using quantitative fluid inclusion gas analysis; Journal of Geochemical Exploration, v. 116-117, p. 17-27.

Bodnar, R.J., 1993. Revised equation and table for determining the freezing point depression of H_2O-NaCl solutions; Geochimica et Cosmochimica Acta, v. 57, p. 683–684.

Carne, R.C., 1979. Geological setting and stratiform lead-zinc-barite mineralization, Tom Claims, Macmillan Pass, Yukon Territory, Canada; Department of Indian and Northern Affairs, Report EGS 1979–4, 30 p.

Czamanske, G.K. and Rye, R.O., 1974. Experimentally determined sulfur isotope fractionations between sphalerite and galena in the temperature range 600ºC to 275ºC; Economic Geology, v. 69, p. 17-25.

Dawson, K.M., and Orchard, M.J., 1982. Regional metallogeny of the northern Cordillera: Biostratigraphy, correlation and metallogenic significance of bedded barite occurrences in eastern Yukon and western District of Mackenzie; Geological Survey of Canada, Paper 82-1C, p. 31–38.

Dickinson, W.R., 2004. Evolution of the North American Cordillera; Annual Review of Earth and Planetary Sciences, v. 32, p. 13-45.

Eisbacher, G.H., 1985. Late Proterozoic rifting, glacial sedimentation and sedimentary cycles in the light of Windermere deposition; Palaeogeography, Palaeoclimatology and Palaeoecology, v. 51, p. 231-254.

Fernandes, N.A., 2011. Geology and geochemistry of Late Devonian-Mississippian sediment-hosted barite sequences of the Selwyn Basin, NWT and Yukon, Canada; Unpublished M.Sc. thesis, University of Alberta, 98 p.

Gabrielse, H., 1967. Tectonic Evolution of the Northern Canadian Cordillera; Canadian Journal of Earth Sciences, v. 4, p. 271-300.

Gardner, H.D., and Hutcheon, I., 1985. Geochemistry, Mineralogy, and Geology of the Jason Pb-Zn Deposits, Macmillan Pass, Yukon, Canada; Economic Geology, v. 80, p. 1257-1276.

Goodfellow, W.D., Lydon, J.W., and Turner, R.J.W., 1993. Geology and genesis of stratiform sediment-hosted (SEDEX) zinc-lead-silver sulphide deposits; Geological Association of Canada, Special Paper 40, p. 201-251.

Goodfellow, W.D., Cecile, M.P., and Leybourne, M.I., 1995. Geochemistry, petrogenesis, and tectonic setting of lower Paleozoic alkali and potassic volcanic rocks, Northern Canadian Cordilleran Miogeocline; Canadian Journal of Earth Sciences, v. 32, p. 1236-1254.

Goodfellow, W.D., 2007. Base metal metallogeny of the Selwyn Basin, Canada; *in* Mineral Deposits of Canada: A synthesis of major deposit-types, district metallogeny, the evolution of geological provinces, and exploration methods, (ed.) Goodfellow, W.D.; Geological Association of Canada, Mineral Deposits Division, Special Publication No. 5, p.553-579.

Goodfellow, W.D., and Lydon, J.W., 2007, Sedimentary exhalative (SEDEX) deposits; *in* Mineral Deposits of Canada: A synthesis of major deposit-types, district metallogeny, the evolution of geological provinces, and exploration methods, (ed.) Goodfellow, W.D.; Geological Association of Canada, Mineral Deposits Division, Special Publication No. 5, p. 163-183.

Gordey, S.P., Abbott, J.G., and Orchard, M.J., 1982. Devono-Mississippian Earn Group and younger in strata in east-central Yukon; Geological Survey of Canada, Current Research, Part B, Paper 82-1B, p. 93-100.

Gordey, S.P. and Anderson, R.G., 1993. Evolution of the northern Cordilleran Miogeocline, Nahanni map area (105I), Yukon and Northwest Territories; Geological Survey of Canada, Memoir 428, 214 p.

Gordey, S.P., Macdonald, J.D., Turner, E.C., and Long, D.G.F., 2010. Chapter 5. Structural geology of the central Mackenzie Mountains; *in* Geology of the central Mackenzie Mountains of the northern Canadian Cordillera, Sekwi Mountain (105P), Mount Eduni (106A), and northwestern Wrigley Lake (95M) map-areas, Northwest Territories, (ed.) Martel, E., Turner, E.C., and Fischer, B.J.; NWT Special Volume 1, NWT Geoscience Office, p. 193-214.

Grassineau, N.V., Mattey, D.P., and Lowry, D., 2001. Sulfur isotope analysis of sulphide and sulphate minerals by continuous flow-isotope ratio mass spectrometry; Analytical Chemistry, v. 73, p. 220-225.

Hart, C.J.R., Goldfarb, R.J., Lewis, L.L., and Mair, J.L., 2004. The northern Cordilleran Mid-Cretaceous plutonic province: ilmenite/magnetite-series granitoids and intrusion-related mineralization; Resource Geology, v. 54, p. 253-280.

Irwin, S.E.B. and Orchard, M.J., 1991. Upper Devonian-Lower Carboniferous conodont biostratigraphy of the Earn Group and overlying units, northern Canadian Cordillera; *in* Ordovician to Triassic Conodont Paleontology of the Canadian Cordillera, (ed.) Orchard, M.J. and McCracken, A.D.; Geological Survey of Canada, Bulletin 417, p. 185-213.

Large, D.E., 1980. On the geology, geochemistry, and genesis of the Tom Pb-Zn-barite deposit, Yukon Territory, Canada; Unpublished Ph.D. thesis, Braunschweig, West Germany, Technische Universität Carolo-Wilhelmina, 152 p.

Longstaffe F.J., 1989. Stable isotopes as tracers in clastic diagenesis; *in* Burial Diagenesis, (ed.) Hutcheon I.E.; Mineralogical Association of Canada Short Course 15, p. 201-277.

Lund, K., 2008. Geometry of the Neoproterozoic and Paleozoic rift margin of western Laurentia: Implications for mineral deposit settings; Geosphere, v. 4, p. 429-444.

Magnall, J.M. and Gleeson, S.A., 2012a. Boundary Creek (Nidd): A preliminary petrographical assessment; Unpublished report – Geological Survey of Canada, 17 p.

Magnall, J.M. and Gleeson, S.A., 2012b. Macmillan Pass – Tom deposit; Unpublished report – Geological Survey of Canada, 14p.

Magnall, J.M., Gleeson, S.A., and Paradis, S., 2014. SEDEX mineralization, Macmillan Pass (Yukon): Petrography, mineralogy and bulk geochemistry of the Tom and Nidd deposits; Geological Survey of Canada, Open File 7457.

Nelson, J., Paradis, S., Christensen, J., and Gabites, J., 2002. Canadian Cordilleran Mississippi Valley-type deposits: A case for Devonian-Mississippian back-arc hydrothermal origin; Economic Geology, v. 97, p. 1013-1036.

Nelson, J., and Colpron, M., 2007. Tectonics and metallogeny of the British Columbia, Yukon and Alaskan Cordillera, 1.8Ga to the present; *in* Mineral Deposits of Canada: A synthesis of major deposit-types, district metallogeny, the evolution of geological provinces, and exploration methods, (ed.) Goodfellow, W.D.; Geological Association of Canada, Mineral Deposits Division, Special Publication No. 5, p. 755-791.

Roedder, E., 1984. Fluid Inclusions; Reviews in Mineralogy, v. 12, (ed.) Ribbe, P.H., Mineralogical Society of America, Washington, D.C.

Thiessen, E.J., Gleeson, S.A., Dufrane, S.A., Carne, R.C., and Dumala, M., 2012. Upper age constraint and paragenesis of the Tiger Zone, Rau property, central Yukon; *in* Yukon Exploration and Geology 2011, (ed.) MacFarlane K.E. and Sack, P.J.; Yukon Geological Survey, p. 151-164.

Turner, R.J.W. and Rhodes, D., 1991. Boundary Creek zinc deposit (Nidd property), Macmillan Pass. Yukon: sub-seafloor sediment-hosted mineralisation associated with volcanism along a late Devonian syndepositional fault; *in* Current Research, Part E, Geological Survey of Canada, Paper 90-1E, p. 321-335

Turner, E.C., Roots, C.F., MacNaughton, R.B., Long, D.G.F., Fischer, B.J., Gordey, S.P., Martel, E., and Pope, M.C., 2011. Stratigraphy; *in* Geology of the central Mackenzie Mountains of the northern Canadian Cordillera, Sekwi Mountain (105P), Mount Eduni (106A), and northwestern Wrigley Lake (95M) map-areas, Northwest Territories, (ed.) Martel, E., Turner, E.C., and Fischer, B.J.; NWT Special Volume 1, NWT Geoscience Office, p. 31–192.

Valley, J.W., 1986. Stable isotope geochemistry of metamorphic rocks; *in* Stable Isotopes in High Temperature Processes, (ed.) Valley J.W., Taylor, H.P.Jr., and O'Neil, J.R.; Mineralogical Society of America, Reviews in Mineralogy, v. 16, p. 445-489.

Veizer, J., Ala, D., Azmy, K., Bruckschen, P., Buhl, D., Bruhn, F., Carden, G., Diener, A., Ebneth, S., Godderis, Y., Jasper, T., Korte, C., Pawellek, F., Podlaha, O., and Strauss, H., 1999. $^{87}Sr/^{86}Sr$, $\delta^{13}C$ and $\delta^{18}O$ evolution of Phanerozoic seawater; Chemical Geology, v. 161, p. 59-88.